Supplementary Information

Phase Selective Synthesis of Cubic WN and Hexagonal WC Carbide via Solid-phase Reaction Pathways Controlling for Electrochemical Applications

Zheng-Hua He [a,b,1], Jian-Fei Gao [a,b,1], Yan-Dong Ma [a,b], Jing-Feng Hou [a,b], Zhe Li [a,b], Ling-Bin Kong [a, b,*]

[a] State Key Laboratory of Advanced Processing and Recycling of Non-ferrous Metals, Lanzhou University of Technology, Lanzhou 730050, P. R. China

[b] School of Materials Science and Engineering, Lanzhou University of Technology, Lanzhou 730050, P. R. China

* Corresponding author. E-mail: konglb@lut.edu.cn

1 These authors contributed equally: Zheng-Hua He, Jian-Fei Gao.

1. Experimental

1.1. Chemicals and materials

All the reagents used in the experiment were of analytical grade and used without further purification. Tungsten trioxide (WO_3, >99%), Dicyandiamide ($C_2H_4N_4$), were purchased from Sinopharm Chemical Reagent Co. Ltd. Deionized water with a resistivity of > 10.0 MΩ was used in experiments.

1.2. Material characterization

Crystal structures of WO_3, WN and WC/C were characterized using X-ray diffraction (XRD, Rigaku, D/MAX2400) with Cu K_α radiation (wave length 0.15418 nm) operating at 40 kV and 60 mA. X-ray photoelectron spectroscopy

(XPS) was recorded by the PHI5702 multi-function electronic energy spectrometer. Morphologies, structures and elemental compositions were monitored by scanning electron microscope (SEM, JEOL JSM-6701F), transmission electron microscope (TEM, JEOL JEM-2010). Energy dispersive spectroscopy (EDS) coupled with SEM is performed for elemental analysis. The thermogravimetric analysis (TGA) of samples was conducted under air atmosphere at a heating rate of 10 °C min^{-1} from 20 °C to 1000 °C using a thermal analyzer (TGA, Netzsch 209F3). The existence of free carbon in tungsten nitride and tungsten carbide was detected by Raman spectrometer (Renishaw invia spectrometer).

1.3. Electrode preparation

The WN and WC/C anodes were prepared by mixing the active material (80 wt.%), super C (10 wt.%), and the binder PVDF (10 wt.%) were mixed in N-methyl pyrrolidone to form slurry, and then the slurry was coated on the clean copper foil collector, followed by drying at 60 °C for 8 h and then transferred to a vacuum drying chamber at 60 °C for 12 h. The mass loading of electrode material coated each circular eletrode was 0.7～1.3 mg.

1.4. Electrochemical evaluation

The electrochemical performance of electrode material was investigated with a cion-type configuration. For half-cells tests, this were assembled using electrode material as anodes and Li foils as reference electrode and counter electrode into a coin cells (CR2032), where the electrolyte was 1.0 M $LiPF_6$ dissolved in EC/EMC/DMC mixture (v/v/v = 1:1:1) and Celgard 2400 as the separator. In this work, the electrode is cut into small round plates with a diameter of 14 mm, and the load of active material on the small round plates is within the range of 0.7-1.3 mg. The cell was done in a glovebox which was full of Ar. The Li-ion hybrid supercapacitor was tested the same as the half cell. All the electrochemicical tests were carried out at room tempperature. Cyclic voltammetry (CV) and galvanostatic charge-discharge (GCD) were recordeed using an electrochemical workstation (CHI660D, shanghai,China). Electrical

impedance spectroscopy (EIS) measurement was measured Autolab (metrohm). The Galvanostatic Intermittent Titration Technique (GITT), cycling charge-discharge test of half-cells and Li-ion hybrid supercapacitor were measured using a CT2001A cell test instrument (LADN Electronic Co.,China).

1.5. Dynamic calculation formula

$$i = a\nu^{b} \quad \text{S1}$$

$$\log(i) = \log(a) + b\log(\nu) \quad \text{S2}$$

In which a is a constant and b is an exponent of power-law. According to the peak of cathode and anode, the slope of log (peak current) vs. log (scan rate) curve is b value. Based on the experimental b value, the dynamics of charge storage mechanism can be qualitatively determined. This is a capacitive behavior when b is 1. When b is 0.5, it is a kind of diffusion control process.

$$i_{(V)} = k_1\nu + k_2\nu^{1/2} \quad \text{S3}$$

$$i_{(V)}/\nu^{1/2} = k_1\nu^{1/2} + k_2 \quad \text{S4}$$

In which k_1 and k_2 represent proportional constants of the pseudocapacitor behavior control and battery behavior control processes, respectively.

$$D = \frac{R^2T^2}{2A^2n^4F^4C^2\sigma^2} \quad \text{S5}$$

$$Z_w = R_e + R_{ct} + \sigma\omega^{-1/2} \quad \text{S6}$$

In which ideal gas constant, absolute temperature, effective surface area of

electrode in lithium-ion battery, transferred charge number, Faraday constant, lithium-ion concentration in the system and Warburg coefficient are expressed by R, T, A, n, F, C and σ respectively.

$$D_{Li^+} = \frac{4}{\pi}\left(\frac{m_B V_M}{M_B S}\right)^2\left(\frac{\Delta E_s}{\tau\left(dE_\tau/d\sqrt{\tau}\right)}\right)^2\left(\tau \ll \frac{L^2}{D_{Li^+}}\right) \quad \text{.....S7}$$

$$D_{Li^+} = \frac{4}{\pi\tau}\left(\frac{m_B V_M}{M_B S}\right)^2\left(\frac{\Delta E_s}{\Delta E_\tau}\right)^2 \quad \text{.....S8}$$

In which V_M, m_B, M_B, S, L, τ, ΔE_s and ΔE_t in the above Equation stand for molar volume, active material weight, molar mass, contact surface area, average thickness of the electrode, relaxation time, the difference of potential change caused by pulse and potential change value during relaxation time, respectively.

1.6. Other related explanations

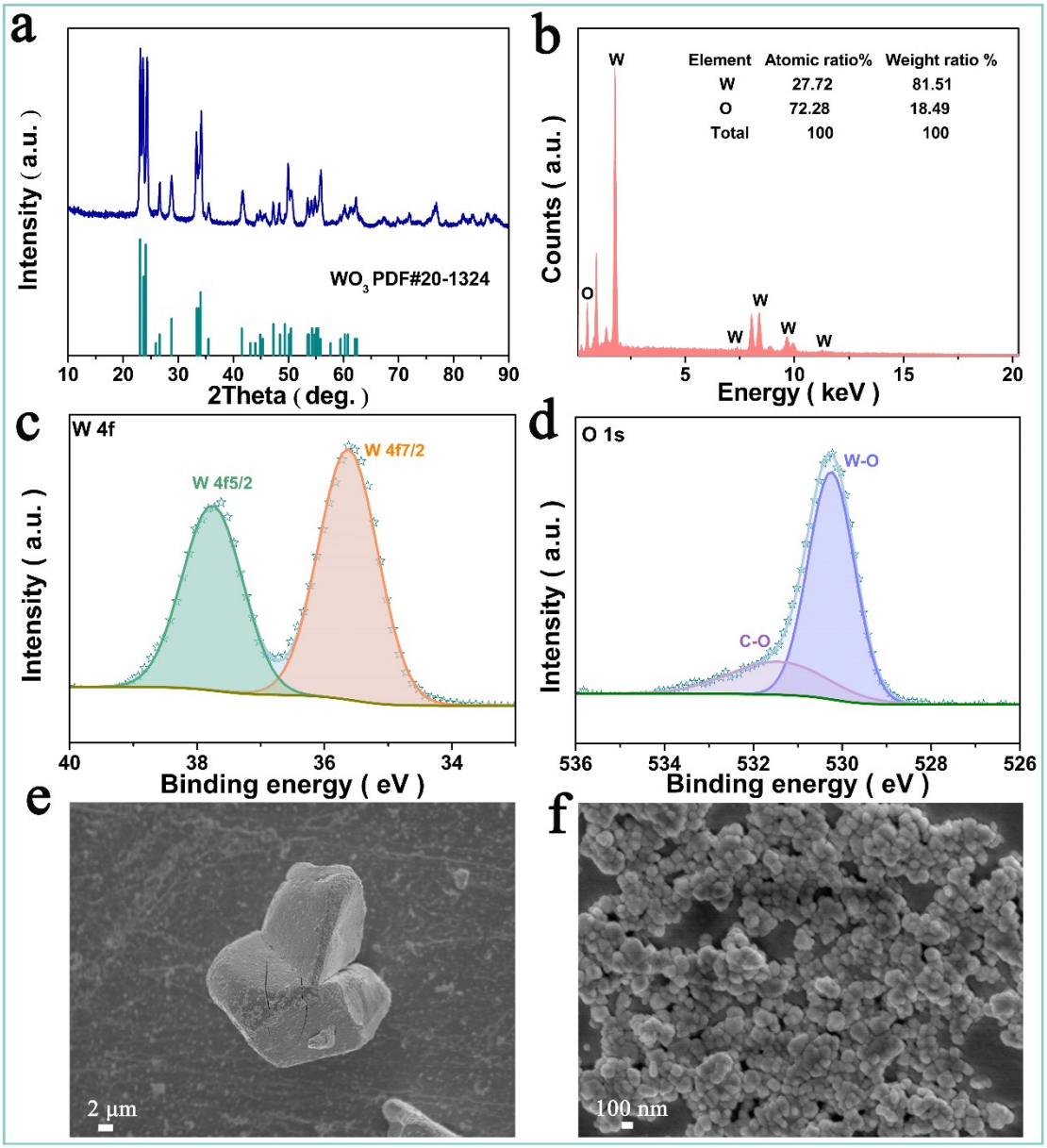

Figure S1. Phase and morphology characterization of the precursor WO_3. (a) XRD; (b) EDS; (c) XPS spectrum of W 4f; (d) O 1s; (e-f) SEM.

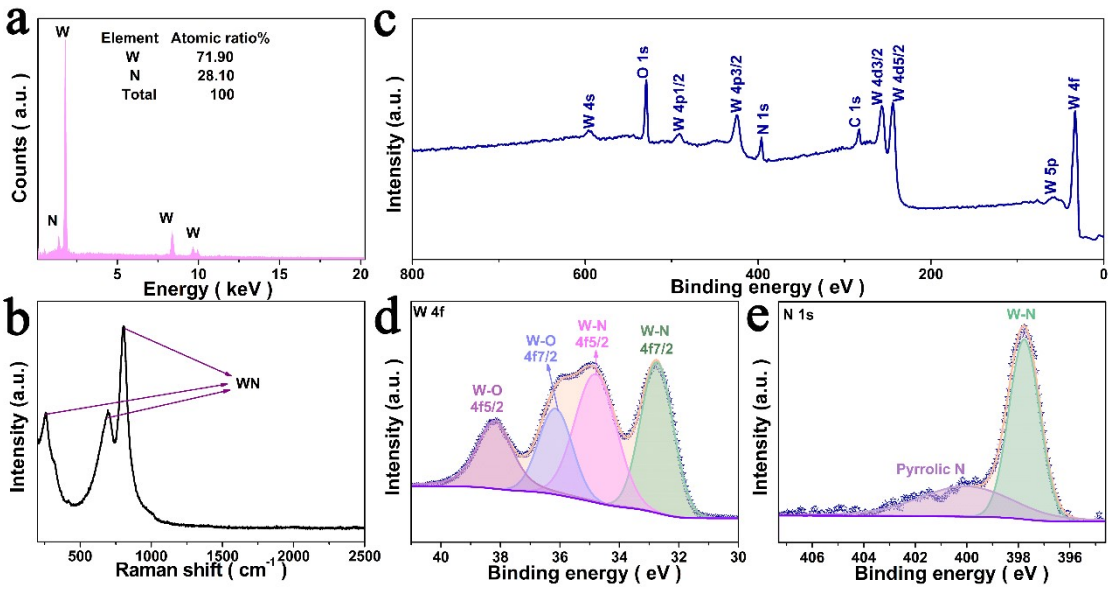

Figure S2. Phase characterization. WN: (a) EDS spectra; (b) Raman scattering; (c) broad-scan XPS; (d) HR W 4f spectra; (e) HR N 1s spectra.

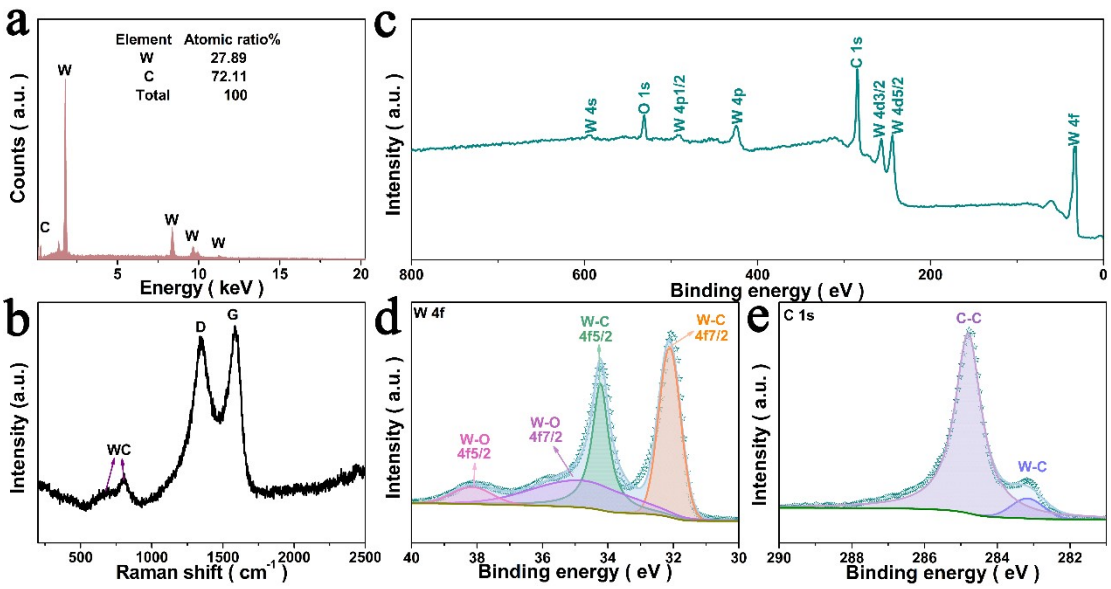

Figure S3. Phase characterization. WC/C: (a) EDS spectra; (b) Raman scattering; (c) broad-scan XPS; (d) HR W 4f spectra; (e) HR C 1s spectra.

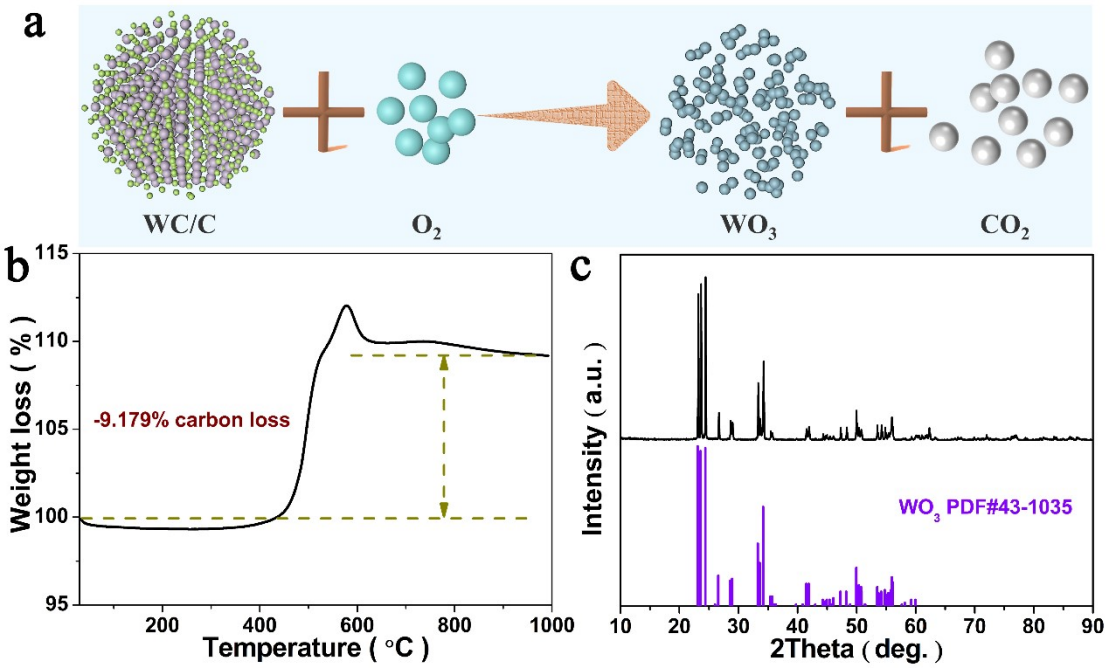

Figure S4. TGA curve of WC/C material: (a) Illustration of the TGA mechanism; (b) TGA curves; (c) XRD of the WC/C after TGA.

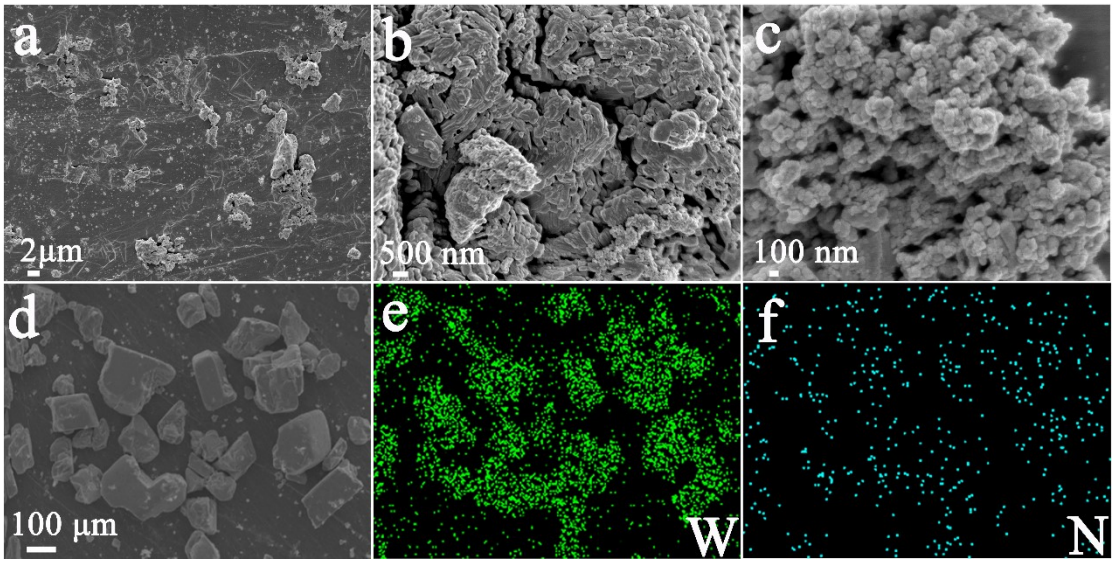

Figure S5. Morphological characterization. WN: (a-c) SEM; (d) EDS mapping: (e) W; (f) N.

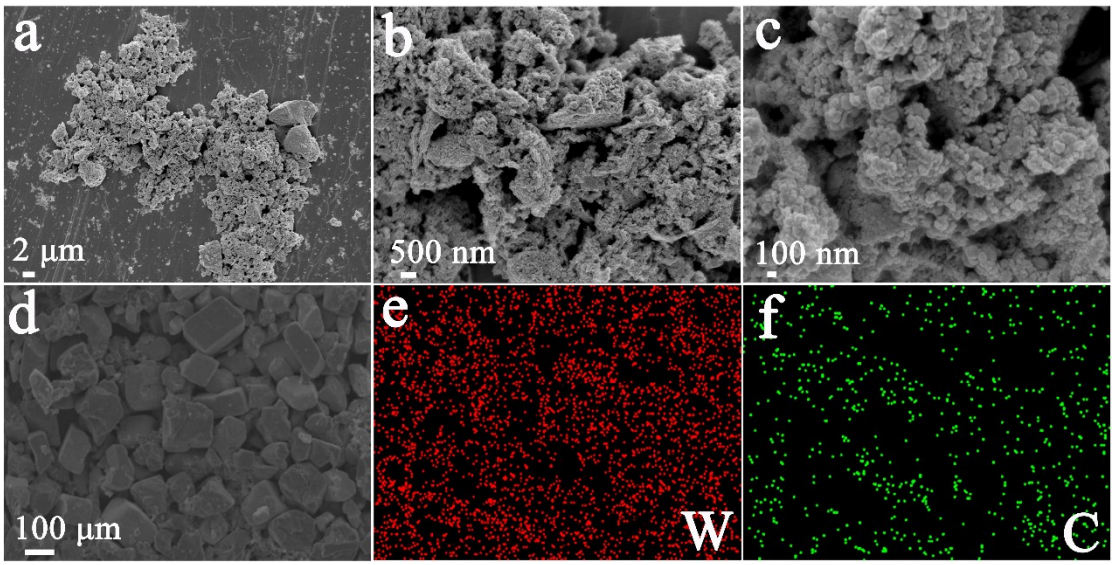

Figure S6. Morphological characterization. WC/C: (a-c) SEM; (d) EDS mapping: (e) W.

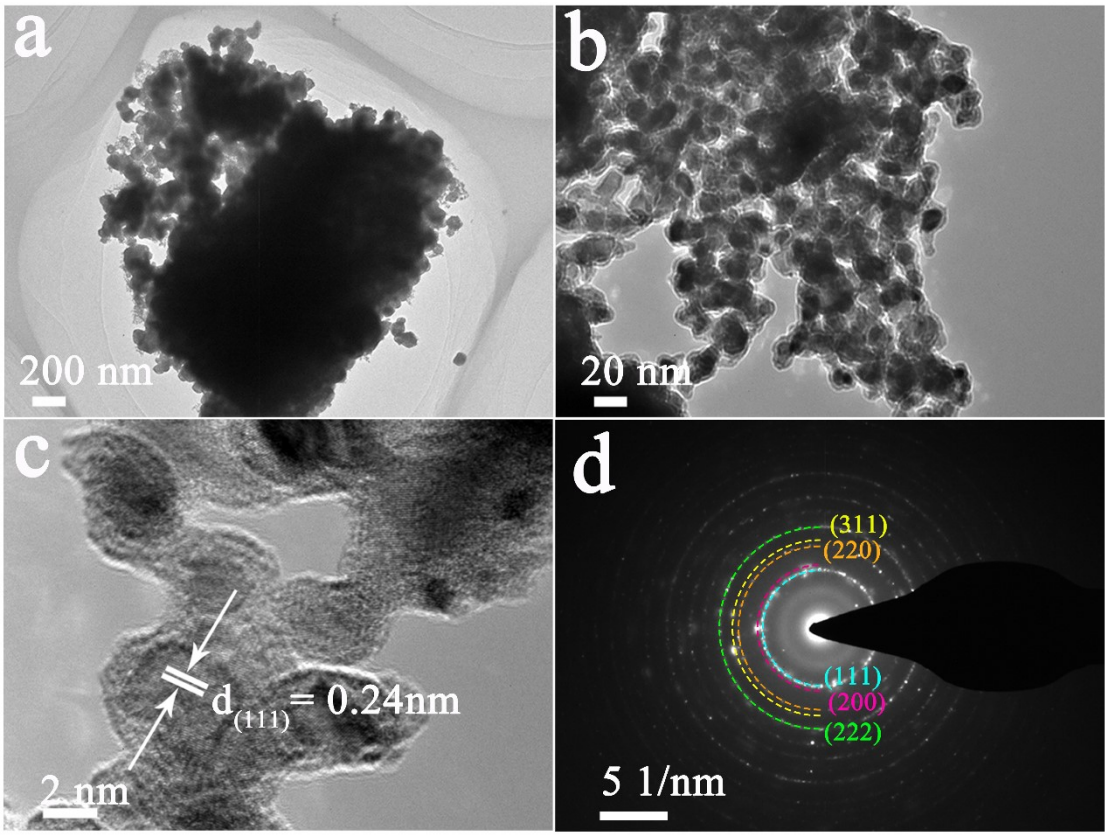

Figure S7. Morphological characterization. WN: (a-b) TEM; (c) HRTEM; (d) SAED.

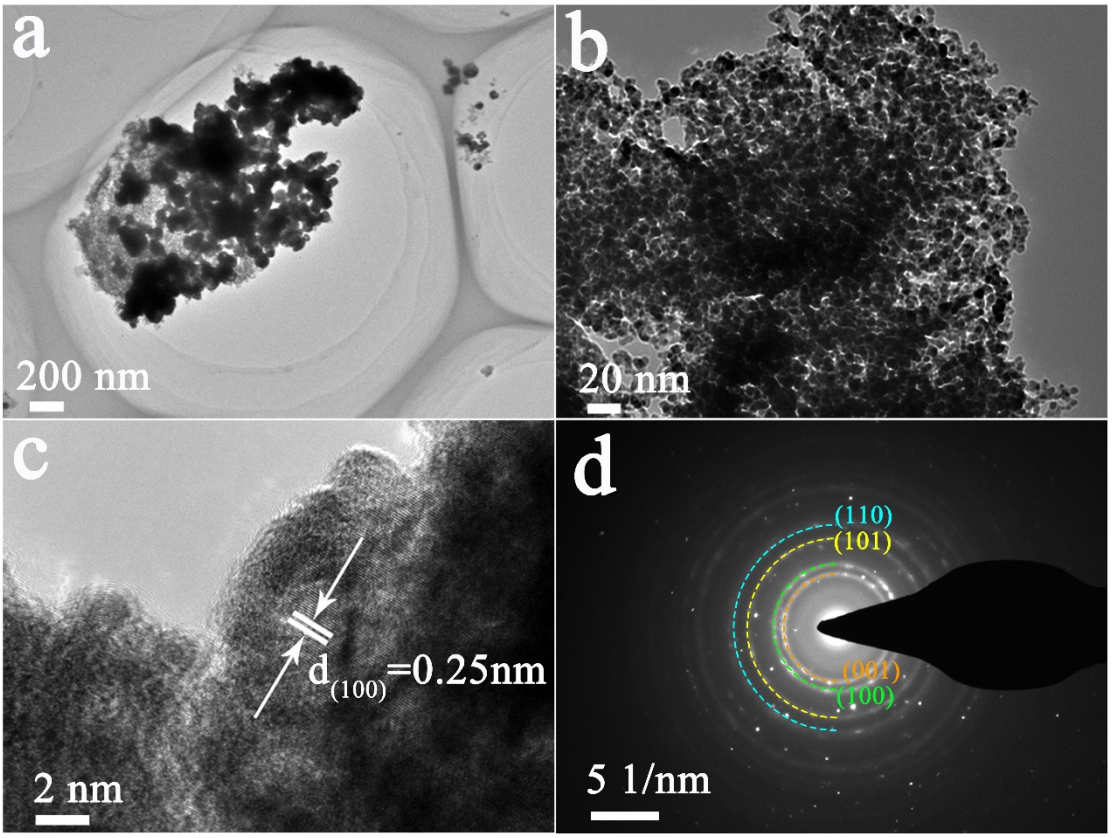

Figure S8. Morphological characterization. WC/C: (a-b) TEM; (c) HRTEM; (d) SAED.

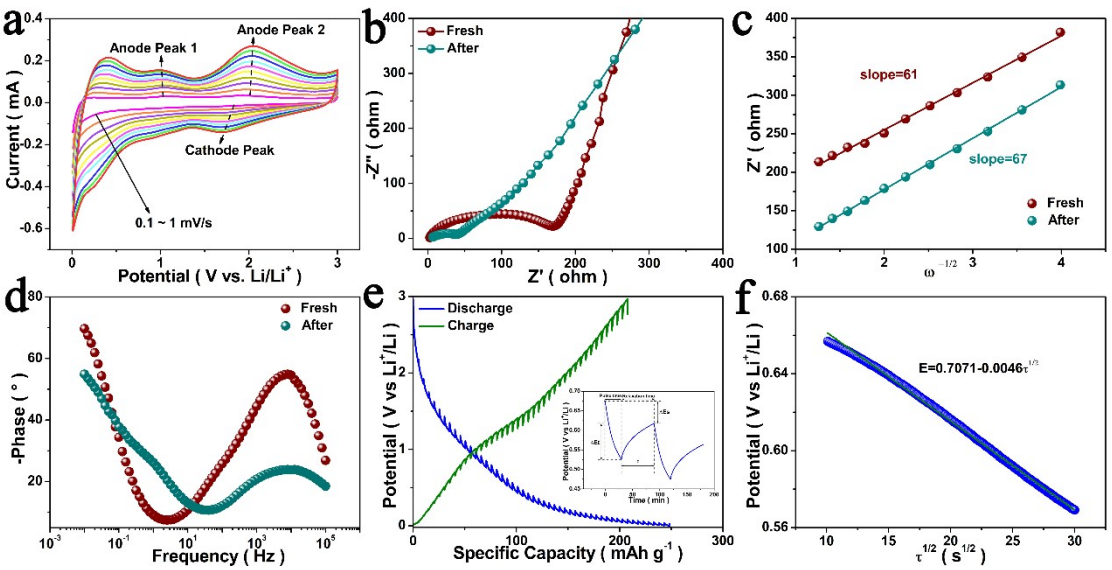

Figure S9. Dynamic investigation of WN. (a) CV; (b) EIS; (c) Warburg analysis; (d) Bode diagrams; (e) GITT, Dual sequential titrations within a selected potential window (inset); (f) $\tau^{1/2}$ vs. V linear fit from a single titration.

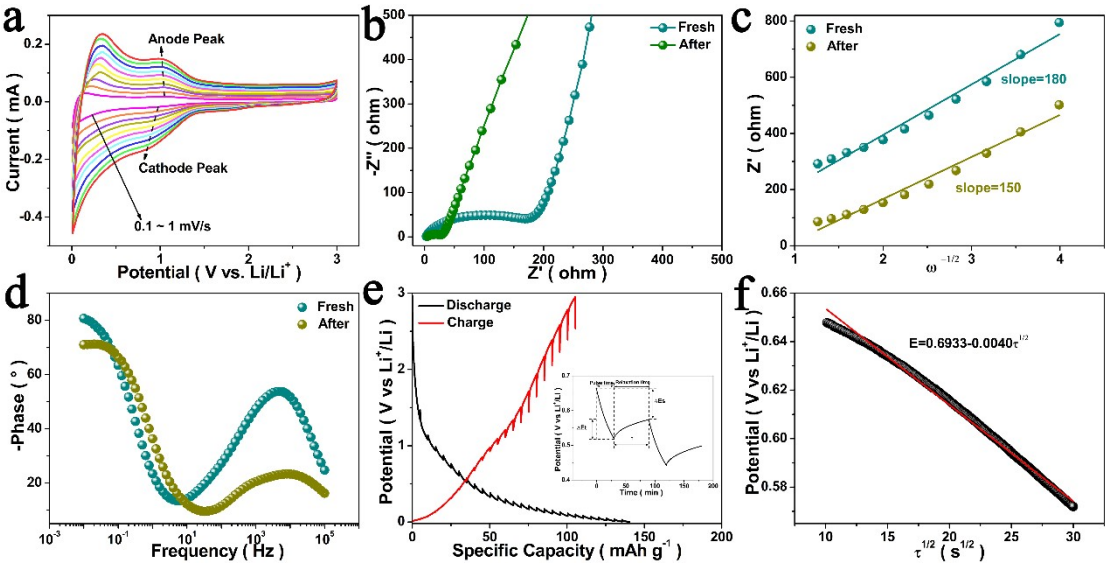

Figure S10. Dynamic investigation of WC/C. (a) CV; (b) EIS; (c) Warburg analysis; (d) Bode diagrams; (e) GITT, Dual sequential titrations within a selected potential window (inset); (f) $\tau^{1/2}$ vs. V linear fit from a single titration.

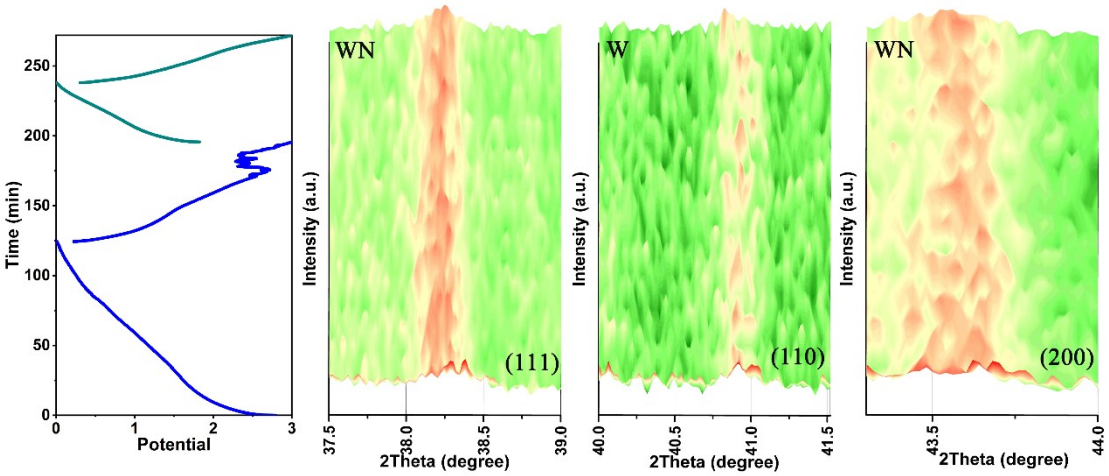

Figure S11. In-situ XRD of WN in the first and second cycles.

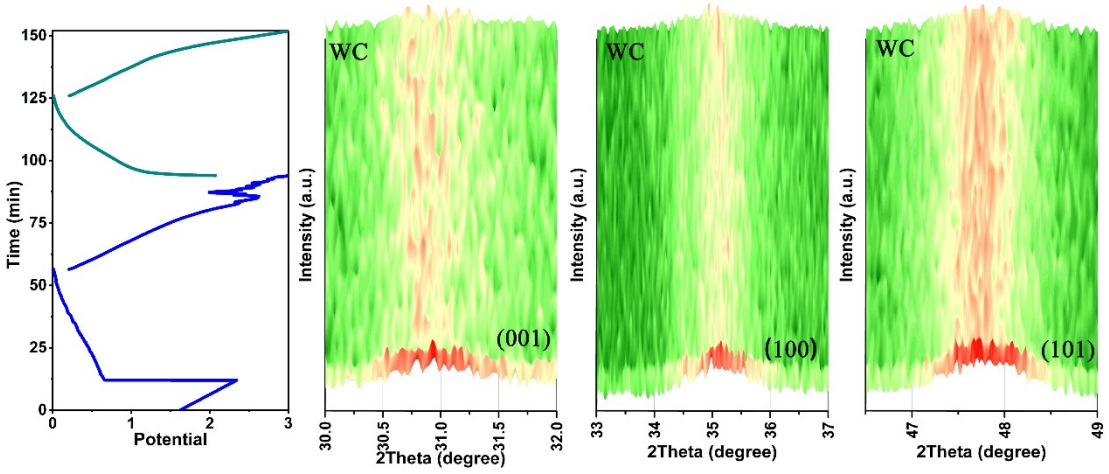

Figure S12. In-situ XRD of WC/C in the first and second cycles.

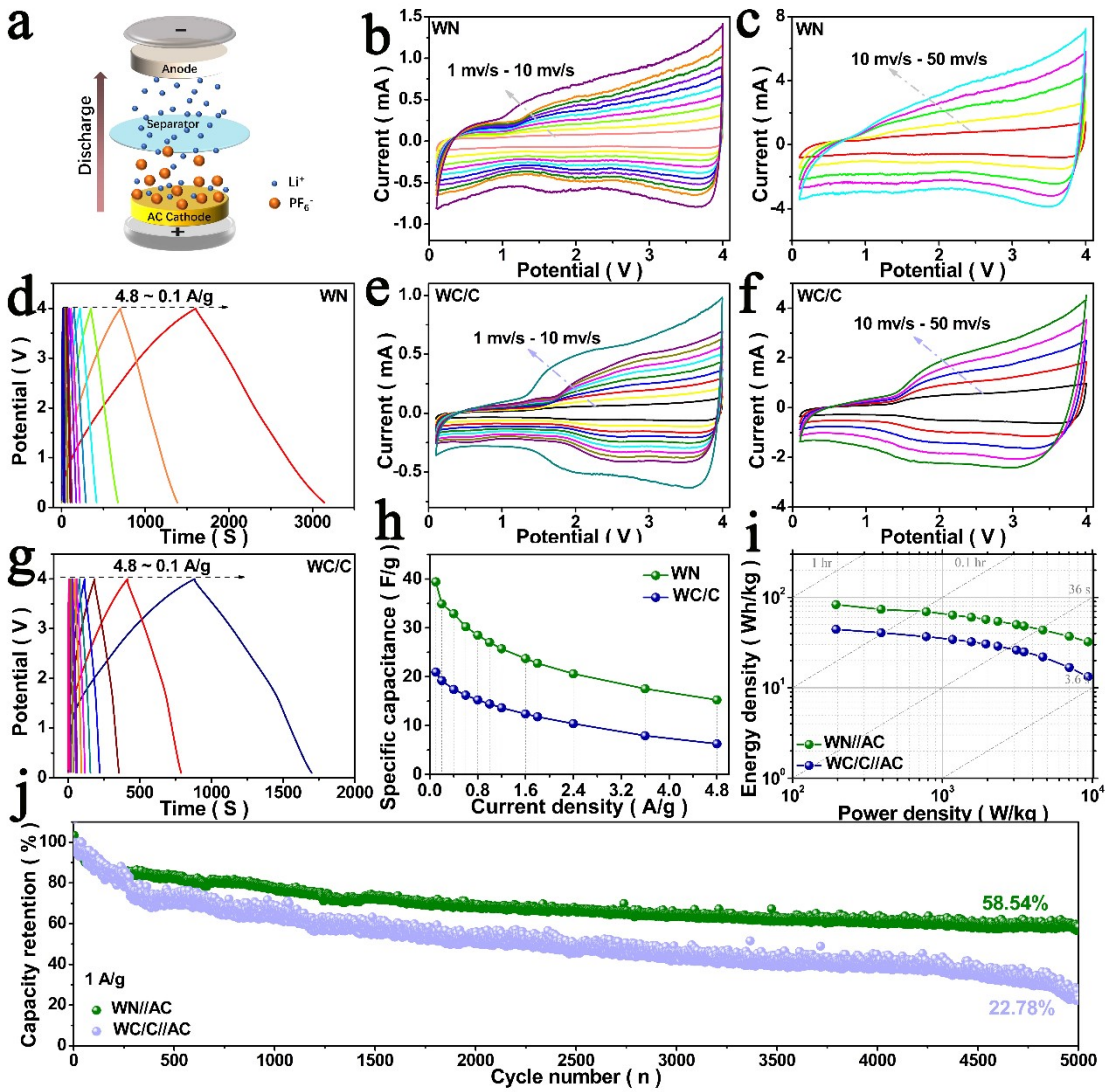

Figure S13. Electrochemical characteristics of WN//AC and WC/C//AC LICs. (a) Working-principle schematic; (b,e) CV recorded at low scan rates; (c,f) CV recorded at high scan rates; (d,g) GCD; (h) capability; (i) Energy-power diagram; (j) Extended cycling stability plot.

Table S1. The cell parameters of WN and WC/C obtained from Rietveld refinement of powder XRD data using GSAS-II.

Samples	a (Å)	b (Å)	c (Å)	V (Å^3)	R_{wp}	R_p	χ^2
WN	4.13903	4.13903	4.13903	70.908078	10.99%	8.72%	1.56
WC/C	2.90410	2.90410	2.83750	20.724766	14.61%	11.19%	2.49

Table S2. Cyclability comparison of as-assembled WN//AC and WC/C//AC LIC with previously reported LICs in literature

LIC Anode//Cathode	Specific capacity (F g^{-1})	Energy density (Wh kg^{-1})	Voltage window (V)	Capacity retention(%)
Fe_3C@DRC//AC[1]	84.5 at 0.1A g^{-1}	187.8 at 200 W kg^{-1}	0-4	84.8-6000 cycles-1 A g^{-1}
p-NbN//APDC[2]	67.2 at 0.1A g^{-1}	149 at 200 W kg^{-1}	0-4	95-15000 cycles-1 A g^{-1}
NbN/GNSs//APDC[3]	65 at 0.1A g^{-1}	136 at 250 W kg^{-1}	1-4	84-2000 cycles-5 A g^{-1}
Mo_2C@NCB//NCB[4]	47 at 0.1A g^{-1}	104 at 200 W kg^{-1}	0-4	80-10000 cycles-5 A g^{-1}
WN//AC	39.41 at 0.1A g^{-1}	83.25 at 195 W kg^{-1}	0.1-4	58.54-5000 cycles-1 A g^{-1}
WC/C//AC	20.95 at 0.1A g^{-1}	44.25 at 195 W kg^{-1}	0.1-4	22.78-5000 cycles-1 A g^{-1}

References

1. J. Li, X. Jin, Y.-X. Hu, C. Lu, Y.-S. Zhang, B.-M. Zhang, L.-B. Kong and M.-C. Liu, *Ionics*, 2020, **26**, 23-31.
2. P. Wang, R. Wang, J. Lang, X. Zhang, Z. Chen and X. Yan, *Journal of Materials Chemistry A*, 2016, **4**, 9760-9766.
3. Z.-K. Chen, J.-W. Lang, L.-Y. Liu and L.-B. Kong, *RSC Advances*, 2017, **7**, 19967-19975.
4. X. Liu, X. Zhang, Y. Dou, P. Mei, X. Ma and Y. Yang, *Chemical Communications*, 2021, **57**, 4966-4969.